

Article

Electrical Resistance Response to Strain in 3D-Printed Conductive Thermoplastic Polyurethane (TPU)

Axel Riddervold ^{1,*} , Ole S. Nesheim ^{1,*} , Sindre W. Eikevåg ^{1,2}  and Martin Steinert ¹ 

¹ Department of Mechanical and Industrial Engineering, Norwegian University of Science and Technology, 7034 Trondheim, Norway; axel.ridder99@gmail.com (A.R.); sindre.w.eikevag@ntnu.no (S.W.E.); martin.steinert@ntnu.no (M.S.)

² School of Electrical, Electronic and Mechanical Engineering, University of Bristol, Bristol BS8 1QU, UK

* Correspondence: ole.s.nesheim@ntnu.no

Abstract: Additive manufacturing (AM) offers new possibilities in soft robotics as materials can easily be combined in multi-material designs. Proper sensing is essential for the soft actuators to interact with the surroundings successfully. By fabricating sensors through AM, sensors can be embedded directly into the components during manufacturing. This paper investigates NinjaTek Eels electrical resistance response to strain and the feasibility of using the material to create strain sensors. Strain sensors were 3D-printed out of NinjaTek Eel, a soft conductive TPU, and was tested during cyclic loading. A custom resistance–strain test rig was developed for measuring sensor behavior. The rig was calibrated for electric resistance, able to measure electric resistance as a function of strain. A parabolic response curve was observed during cyclic loading, which led to ambiguous readings. A 10-specimen validation test was conducted, evaluating the statistical variation for the first 100 loading cycles. The validation test showed that the sensor is capable of accurate and predictable readings during single load cases and cyclic loading, with the overall root mean square error being 66.9 Ω. Combining two sensors of different cross-sections gave promising results in terms of calibrating. By monitoring load cycles and strain rates, calibration can also be achieved by machine learning models by the microcontroller used to extract data. The presented work in this article explores the potential of using conductive TPUs as sensors embedded in products such as soft robotics, life monitoring of products with structural, and digital twins for live product to user feedback.

Keywords: flexible and stretchable sensors; printable sensors; additive manufacturing; soft robotics sensors



Citation: Riddervold, A.; Nesheim, O.S.; Eikevåg, S.W.; Steinert, M. Electrical Resistance Response to Strain in 3D-Printed Conductive Thermoplastic Polyurethane (TPU). *Appl. Sci.* **2024**, *14*, 3681. <https://doi.org/10.3390/app14093681>

Academic Editors: Carlos Miguel Santos Vicente and Marco Leite

Received: 15 March 2024

Revised: 19 April 2024

Accepted: 23 April 2024

Published: 26 April 2024



Copyright: © 2024 by the authors. Licensee MDPI, Basel, Switzerland. This article is an open access article distributed under the terms and conditions of the Creative Commons Attribution (CC BY) license (<https://creativecommons.org/licenses/by/4.0/>).

1. Introduction

Soft robots are flexible actuators designed to adapt, deform, and comply to complex environments, conforming to surfaces and the environment while avoiding rigidity and stiffness [1–3]. Soft technologies have gained significant attention due to their potential applications in a variety of fields, including medical devices, human interacting robotics, and industrial applications [4,5]. The main actuation technologies are pneumatic, shape memory materials, electroactive, magnetic, and chemical [2,4,6,7]. Pneumatic soft actuators, made of compliant materials, require complex geometries to transfer pressure into actuation and stiffening [8–11]. Actuators are often casted in complex procedures combining several components with multi-stage casting to create the required geometrical structures [8,10,12–18].

Additive manufacturing (AM) and fused filament fabrication (FFF) allows for the fabrication of components by extruding thermoplastic filament into a solidifying geometry [19–21]. Availability, simplicity, design flexibility, and affordability have made AM a common soft robotics mold fabrication method for elastomer casting [8,10,12–14,16–18]. However, AM and FFF also introduces design freedom compared to casting processes, allowing for single-step fabrication with internal structures, thin walls, minimal volume

compartments, and complex geometries [3,5,22]. Multimaterial printing with conductive materials allows for new innovative smart products with embedded sensors that allows for strain, pressure, temperature, and humidity detection [23]. In addition, FFF offers the option to fabricate complex, all-in-one, and low-cost actuators out of TPE and TPU in a single step process [22,24–28].

In biomechanical applications, recent studies show sensors capable of measuring body movements, joint bending motions, phonations, and cardiac activities [29]. There has also been a development in 3D-printed nanostructures that allow for the mechanical sensing of products [30]. Sensors embedded into products with different functionalities and using different materials is a promising research direction [29], and we suggest that the next step is to embed sensors into any material or product. The layer-by-layer building process in additive manufacturing (Figure 1A) allows for the implementation of embedded sensors within the products that are capable of in situ monitoring. Implementing sensors by conductive filament is applicable to any product if it is capable of accurately sensing. Examples of sensor-embedded products can be soft robotics with large deformations, products with structural integrity for end-of-life monitoring, and digital twins where the product can provide live feedback. Due to the process of multi-material printing, the embedded sensor may be implemented independently of component complexity and can be designed in the X, Y, and Z dimensions. The embedding of the sensor by FFF can be seen in Figure 1A, and a hypothetical example of a sensor embedded in a soft robotic gripper arm gripping a strawberry is shown in Figure 1B.

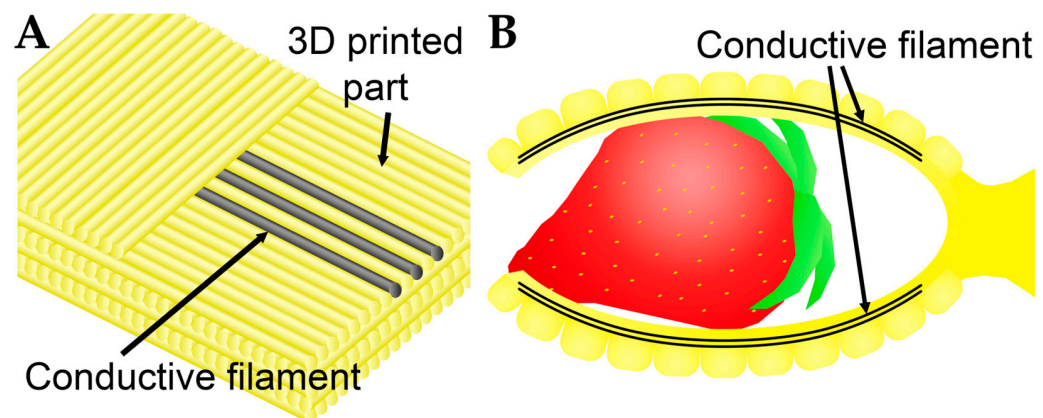


Figure 1. Multimaterial printing with conductive filament potential, (A) conductive filament printed into 3D-printed part, and (B) hypothetical soft robotics gripper application.

AM also introduces the possibility to easily manipulate compliance by fabricating multi-material and meta-material components or by integrating other features such as self-healing in the structure [2,25,31,32]. NinjaTek Eel [33] is a commercially available TPU 3D-printing filament with carbon additives, resulting in both conductive and flexible properties [34]. The material can be integrated in the component to create integrated PCBs and three-dimensional meshes of flexible conductive wires.

To ensure the suitable and autonomous behavior of an actuator, it is important to be aware of the surrounding environment and gather information [35]. Soft sensors can accurately capture information about the environment while also maintaining compliance [36,37]. Typically, flexible sensors are fabricated by reducing the geometric dimension in one or more axes, allowing for compliance [38]. Printed sensors have been used to measure strain, tactility, pressure, stress, displacement, acceleration, magnetic fields, temperature, and humidity [39–42]. FFF offers the possibility to print flexible sensors integrated into soft robots using multi-material printing, although previous studies have shown the working concept utilizing stiffer materials, such as conductive PLA [26]. A softer conductive material may lead to a more compliant component. Previous studies has shown that TPU has excellent toughness and cyclic fatigue resistance [43], making TPU a possible

sensor material. We can measure responses to stimuli of the component by integrating meshes on NinjaTek Eel directly into the components. Previous studies have concluded that NinjaTek Eel is unsuitable for strain sensing applications as a secondary peak is observed in the strain response [44].

Most strain measurements are performed using stress–strain test equipment, often referred to as universal test machines. These are typically designed for force measurements and cannot be used for measuring electric resistance in the specimen, requiring development of a custom test rig. Stepper motors are suitable for such applications, as they are capable of accurate and precise actuation in open-loop systems [45]. In this paper, we present data showing NinjaTek Eels' electric resistance response to strain, allowing for integrated strain sensing in soft robots.

2. Materials and Methods

2.1. Sensor Evaluation Methods

NinjaTek Eel test specimens were printed on a Prusa i3 MK2S FFF 3D-Printer (Prusa Research, Prague, Czech Republic). Print parameters used to fabricate the test specimens can be seen in Table 1. The geometry of the specimens can be seen in Table 2. The specimens were printed with the length and width in the x-y plane. The fabrication parameters were chosen based on trial and error as there exist no acceptable printing guidelines for printing NinjaTek Eel.

Table 1. Fabrication parameters.

Parameter	Value
Printer	Prusa i3 MK2S
Slicer	PrusaSlicer-2.5.1
Nozzle Diameter	0.6 mm
Nozzle temperature	238 °C
Bed Temperature	50 °C
Extrusion Multiplier	1
Max Volumetric Flow	1 mm ³ /s
Part Cooling Fan Speed	100%
Layer Height	0.2 mm

Table 2. Specimen geometry.

Dimension	Value
Length	120 mm
Width	1.2 mm
Height	2 mm
Cross-Section Area	2.4 mm ²

A custom test rig, as seen in Figure 2, was developed to evaluate the electrical resistance response to strain. The setup consisted of two NEMA 17 stepper motors with lead screws driven by an Arduino Uno and an Arduino Motor Shield (Arduino, Turin, Italy). To measure the electric resistance, the Arduino Uno was set up to measure the current over a known resistance and the specimen.

To validate the electrical resistance measurement in the test rig, resistors with known resistances were measured with a multimeter and placed in the test rig. The resistors with verified resistances of 4.16, 5.56, and 21.8 kΩ were measured to 4.11, 5.49, and 21.8 kΩ, respectively, indicating that the test rig is capable of accurately measuring the resistance.

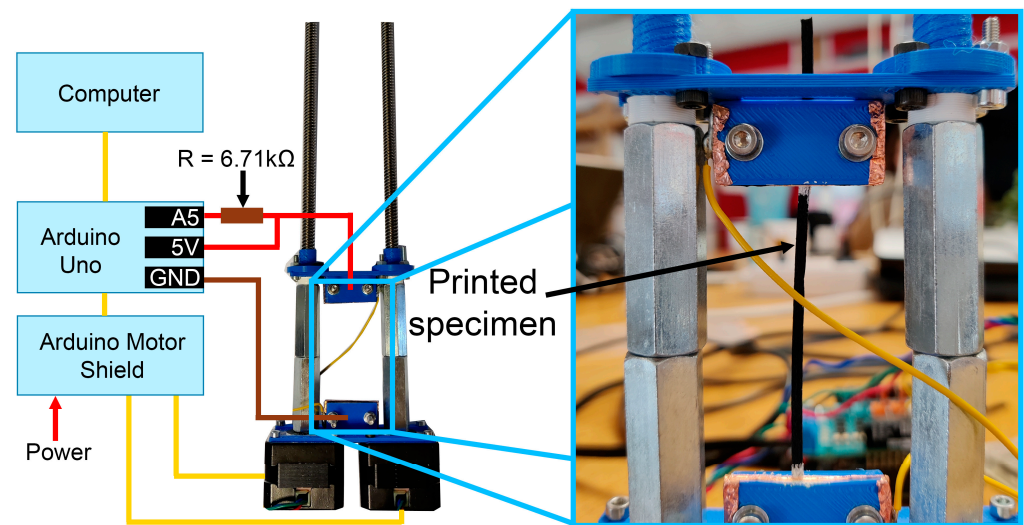


Figure 2. Test rig setup used to measure cyclic strain rate and electrical response.

To evaluate the electric resistance response to strain, a variation in tests was conducted to observe the behavior in different situations. The following tests were conducted:

- Cyclic loading test—1000 cycles of strain were applied to the sensor. The sensor was strained to a strain of 0.5 at a strain rate of 0.306 s^{-1} before being unloaded again.
- Initial cycle and strain rate test—The sensors were cyclically strained to a strain of 0.05, 0.1, 0.2, 0.5, and 1 before being unloaded, i.e., within the elastic region of the material [33]. This was carried out for 3 different strain rates; 0.306 , 0.037 , and 0.015 s^{-1} .
- Validation test—10 samples of the sensor were strained for 100 cycles up to a strain of 0.5 at a strain rate of 0.307 s^{-1} .
- Creep—The sensor was strained to 1 and maintained for 15 s before unloading the sensor and letting it rest for 15 s. This was carried out to evaluate any creeps in the sensor. The test was performed at a strain rate of 0.306 s^{-1} .

2.2. Calibration Attempts

Based on the results in Section 3.1, two attempts were performed to calibrate the sensor. The main objective of this calibration was to evaluate the potential implementation of printed sensors for end use applications. A functional sensor should be unambiguous. Given a resistance measurement, the output of the sensor should correspond to a singular strain value. However, due to the parabolic shape of the strain–resistance curve in Figure 3B (i.e., hysteresis in the strain response), two corresponding strain values for every resistance value were observed. To achieve unambiguity, the proposed sensor setup should avoid the minimum value or introduce features that exclude one of the possible strain values. Compensation for this hysteresis response was, therefore, attempted by pre-straining the sensor and maintaining a strain window within the strictly sinking values, for strains smaller than the observed minimum. This was conducted for two strain windows: 0.15–0.25 and 0.15–0.2. Another attempt at fixing this issue consisted of comparing two sensors with different cross-section areas. If resulting in different strains, then the two values may be combined to determine one unambiguous reading. The sensor couple was strained cyclically to a strain of 0.5. All attempts were tested with a strain rate of 0.307 s^{-1} .

3. Results

3.1. Electric Resistance Response Results

The Ninjatek Eel FFF sensor shows a predictable and consistent behavior during cyclic strain (Figure 3A). A secondary peak can be observed in the strain response.

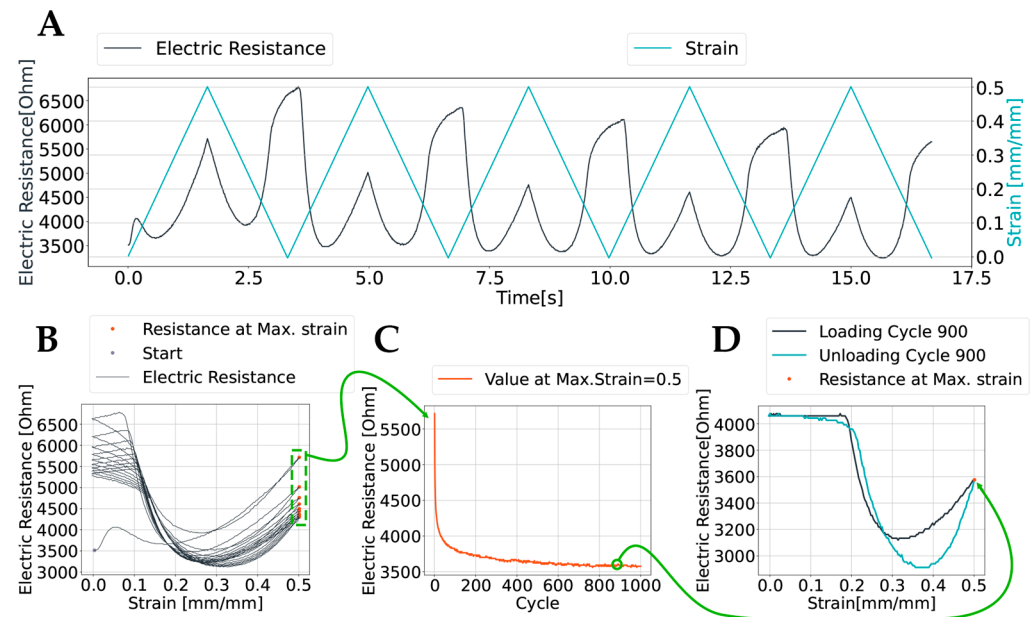


Figure 3. Electric resistance response to strain; (A) electric resistance during cyclic load as a function of time; (B) parabolic electric resistance during cyclic load as a function of strain; (C) electric resistance at max. strain trend over multiple cycles of straining; (D) electric resistance over strain at close to steady state. The green arrow between (B) and (C) indicates how the curve in (C) is derived from the points in (B). The green arrow between (C) and (D) indicates the maximum strain at cycle 900.

Figure 3B shows the raw data output of resistance over strain and how the peak strains plotted in Figure 3C were derived. The behavior during cyclic load is variable for the first number of loading cycles (Figure 3B) but converges towards a close to steady-state behavior (Figure 3C) with a repeatable and predictable response (Figure 3D). The initial loading cycle results in an increased resistance at 0 strain, also resulting in an increased resistance throughout the cycle, which drops off as the number of cycles increases.

Figure 4 shows the electric resistance response during the initial loading cycle.

The initial loading cycle deviates significantly from the later response. This behavior is, however, also repeatable and predictable. Figure 4 shows that the initial strain response follows the same curve shape for all tested strain rates up to a strain of 0.5. This is evident when comparing the initial loading cycles up against each other. They follow the same curve with a small peak before increasing. The maximum strain does, however, affect the relapsing when unloaded. All the plots in Figure 4 relapses to different electrical resistance values although they follow a trend where they drop to a minimum. When reaching a strain of 0.5, the strain rate influences the behavior, yielding an increase in the resistance for the specimens with larger strains (Figure 4E).

The results from the validation test, seen in Figure 5, show that there is little variation between the specimens. For the 10 specimens, the largest standard deviation was 110.9 Ω at cycle 1. The standard deviation was 58.0 Ω at cycle 100. The overall root mean square error (RMSE) for all 10 specimens was calculated to be 66.9 Ω . Within the tested 100 cycles, the 10 specimens follow the same curve and show similar behavior. The standard deviation appears to result from the difference in initial electric resistance prior to loading.

The sensor is additionally subject to creep. As seen in Figure 6A, the resistance drops off as a function of time when constant strain is applied. This is also the case during relaxation. It is, however, clear that the creep phenomenon converges with time (Figure 6B).

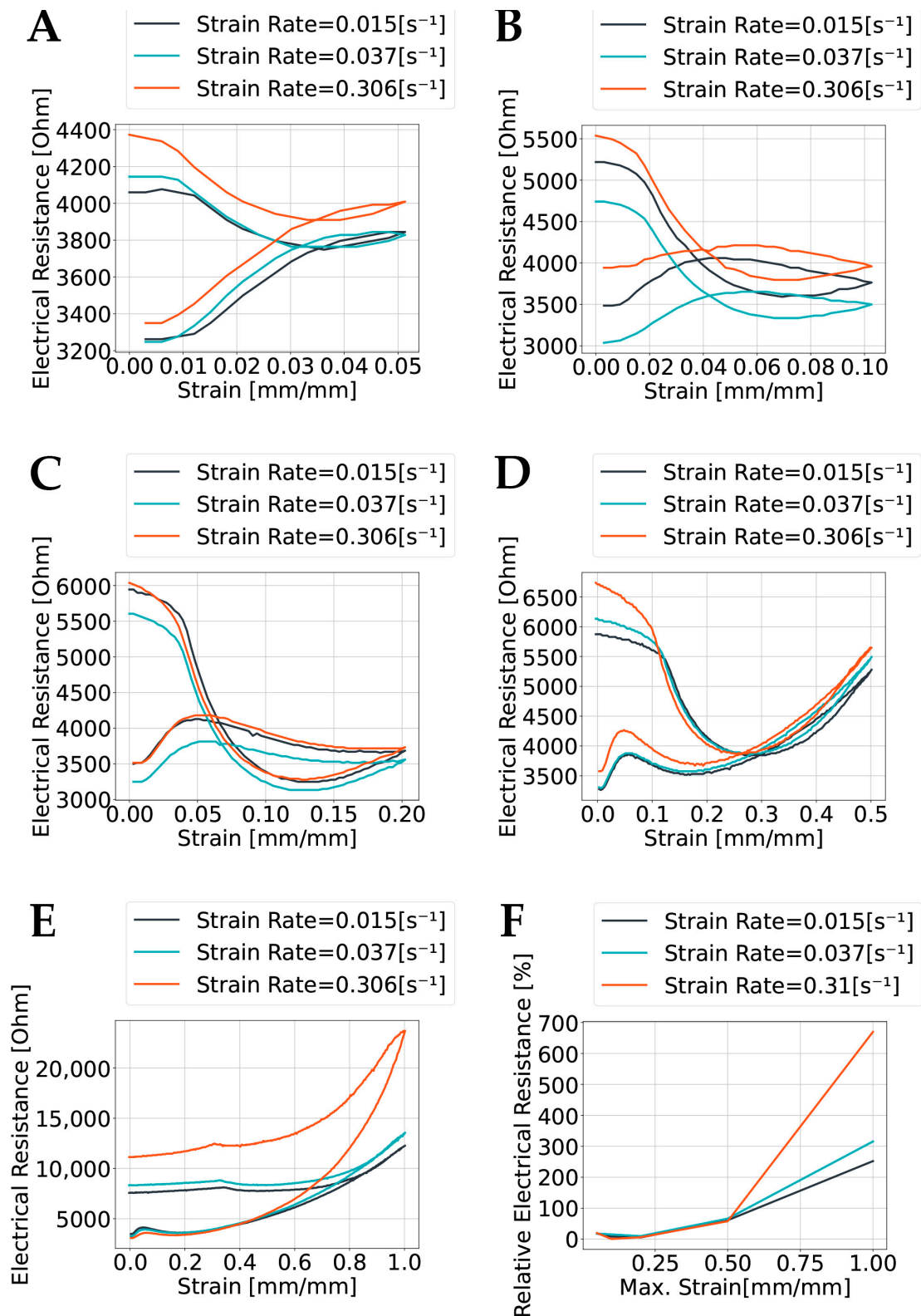


Figure 4. Electric resistance response during the initial cyclic loading: (A) max. strain = 0.05; (B) max. strain = 0.1; (C) max. strain = 0.2; (D) max. strain = 0.5; (E) max. strain = 1; (F) relative increase in electrical resistance during initial loading cycle for different strain rates.

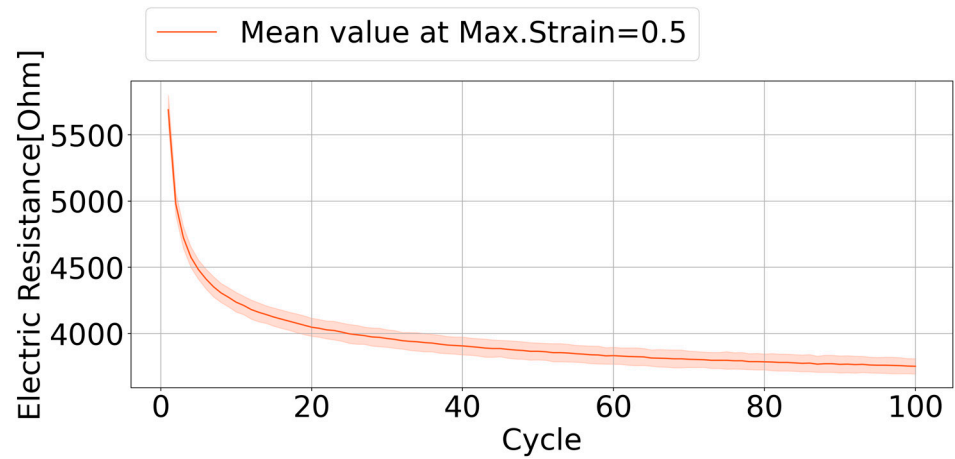


Figure 5. Validation test. Mean value at max strain. Standard deviation plotted as shadow. N = 10.

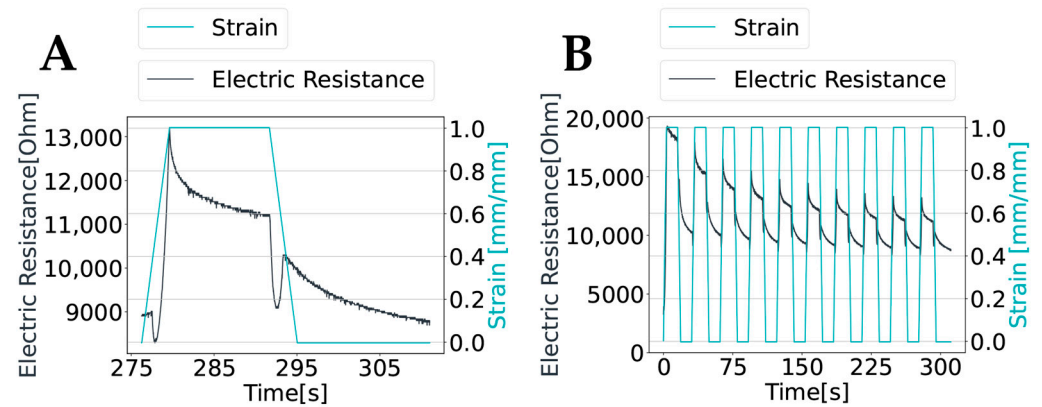


Figure 6. Creep behavior: (A) creep behavior during cyclic load; (B) creep behavior during loading cycle 10.

3.2. Calibration Attempts

The calibration attempts can be seen in Figure 7.

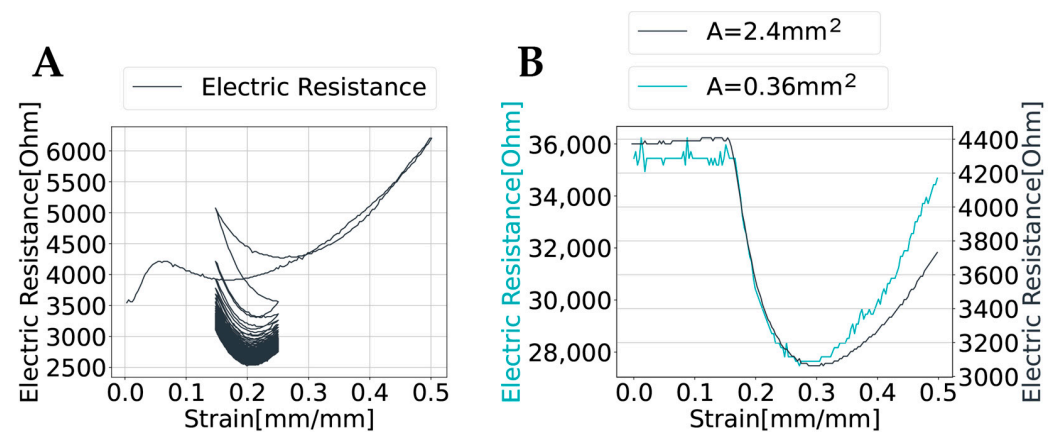


Figure 7. Calibration attempts: (A) resistance response for pre-strained specimen cyclically loaded within a strain window of 0.15–0.25; (B) resistance response for specimens with a difference in cross-section area.

In Figure 7A, the pre-strained specimen reshaped into a new parabolic curve inside the strain window where the electric resistance was previously observed to be strictly sinking with strain in Figure 3B. While the minimum value was observed to be outside of the strain

window in Figure 3B, it moves into the strain window in Figure 7, creating new ambiguous readings. Regarding the attempt to use two specimens with different cross-section areas to extract an unambiguous strain (Figure 7B), the specimens showed a similar behavior. There was, however, a slight discrepancy between the two different cross-sections after a strain of 0.3, even though the signal before 0.3 are very similar. In this region, the sample with the smallest cross-section reads a higher resistance than the other specimen.

4. Discussion

The results show a systematic and predictable correlation between strain and the electric resistance after the initial loading cycle. When observing the time dependent behavior, a secondary peak can clearly be observed, as previously reported by Georgopoulou et al. [44]. The sensors do, however, show a repeatable parabolic strain dependent behavior after the initial loading cycle. As strain is applied, the electric resistance is reduced before the resistance increases with the strain. This repeatable behavior makes the material suitable for strain sensing applications, as the strain can be derived from the electric resistance. However, hysteresis is present, and a calibration model should consider the different responses during loading and unloading. This could complicate applications significantly.

Based on the converging behavior, the material maintains its strain-sensing capabilities for a significant number of loading cycles. After approximately 250 loading cycles, the cyclic behavior seems to have reached a close to steady-state condition where drift is negligible. From this point, the sensor would be able to accurately give information about the current cyclic strain. It is reasonable to believe that this behavior could be maintained until fatigue failure occurs. Previous studies have shown that TPUs show excellent toughness and cyclic fatigue resistance, indicating that the material is suitable for cyclic loading cases [43].

For the 10-sample validation test, there is a small standard deviation in the convergence. They follow the same converging pattern, indicating that different sensors will be able to yield similar behavior. There would only be a small difference from sensor to sensor. Based on Figure 5, the standard deviation looks to be mainly a consequence of a difference in initial resistance. One might, therefore, be able to calibrate the sensor based only on the initial electrical resistance measured prior to loading.

The sensor could also be suitable for measuring strains during the initial loading. As seen in Figure 4, the electric resistance response follows the same curve for all strains and is independent from the strain rate up to a strain of 0.5. One could, therefore, use the sensors in applications requiring strain measurements up to a strain of 0.5 without considering the strain rate. One should, however, take creep into consideration when using the sensor for applications. The sensor shows a significant degree of creep, with a substantial change in resistance during the first seconds after strain is applied. This might be a problematic feature when designing a calibration model for the sensor.

As the sensor is fabricated with FFF, the sensors can be printed directly integrated into the actuators in the single-step fabrication. FFF has already shown itself to be a proven fabrication method for soft robots. NinjaTek Eel requires no extra equipment for printing. The sensors could, therefore, be printed into the structure using a multi-material compatible 3D printer, allowing for complex webs and geometries of strain sensing sensors. Continuing this research may make part monitoring in 3D-printed components easier, enabling lifetime and component failure prediction. This applies not only to soft robotic applications but also to more rigid components.

A soft robotics sensor application requires an external microcontroller for calculating the strain based on the electric resistance. The data presented in this paper show that the sensor reaches a close to steady-state behavior after approximately 250 loading cycles and follows a repeatable behavior both before and after this point. It may, therefore, be possible to calibrate the sensor through a “pre-activation” phase of minimum 250 cycles before use; however, this may be highly impractical in actual application. Since the microcontroller would continuously monitor the sensor load case, an alternative to this solution is to extract

an accurate strain already after the first loading cycle by calibrating the microcontroller for the predictable and repeatable sensor drift shown in Figure 5.

Both calibration attempts presented in Section 2.2 were performed with the aim of fixing the ambiguity issue arising from the polymeric behavior of the resistance–strain curve. The attempts of pre-straining the sensor was unable to achieve this goal as a new parabolic curve emerged. This result simply created the same problem over again. However, the attempts of utilizing sensors with a difference in cross-section area gave potentially promising readings as a slight discrepancy between the two sensors occurred after a strain of 0.3, marking the parabolic curve minimum. This may be used for separating the readings before the curve minimum from after. The sensor sensitivity should also be calculated after a successful setup and calibration has been achieved. This should be conducted for the sake of the user and to compare the sensor with other work.

Other solutions than the two presented in Section 2.2 are combining multiple angled sensors in a full bridge strain gauge setup to be able to extract an unambiguous strain value from the electric resistance response [46]. Also, the sensor may be combined with other sensors and trained using a machine learning algorithm. In addition, the sensor may still be used for other applications, such as a binary sensor generating an active/non-active response.

There may be multiple factors affecting the sensor behavior that have not been identified. All tests were conducted with a voltage of 5 V. Variations in voltages and currents have not been tested. It is also possible that temperature may affect the resistance of the sensor. Furthermore, the tests have been restricted to cyclic testing, and we do not know the effect of more arbitrary strains on the sensor behavior. It is, however, not unlikely that this will drastically affect the sensor useability as the sensor is susceptible to both hysteresis and curve reshaping, as shown in Figure 7A.

By adding sensors to products, we argue that smart components capable of providing user feedback, monitoring, and input for soft robotics could have a major impact on product development. In the process of FFF, now with an increasing availability of multi-material hardware, such sensors can be embedded internally into such components. The FFF process allows for three-dimensional sensor integration with no restrictions in terms of product complexity. FFF is also an excellent manufacturing method for products with complex geometries and specialized components with custom interfaces, and our proposed research is the first step in adding sensing capabilities into such products with relatively low effort and cost. In summary, we argue that the combination of conductive filament and the FFF process will enable sensing in products without a major increase in cost and, therefore, have a major impact on smart product designs.

5. Conclusions

Three-dimensionally printed sensors printed in NinjaTek Eel shows a repeatable, predictable, and usable electric resistance response to strain and can potentially be integrated by FFF into components. During cyclic loading, the sensor outputs accurate and stable readings. The RMSE was calculated to 66.9Ω , with the deviation being most prominent in the first loading cycle. The results indicate that the measurement deviations are mainly an effect of initial resistance variations occurring prior to loading. This makes it suitable for soft robotics applications, given a functional calibration model is in place. By combining multiple sensors with various cross-sections, we have achieved promising results in terms of calibrating for a change in the hysteresis loop. The sensor might also be calibrated by monitoring load cycles and strain rates by implementing machine learning models to the microcontroller used to extract data. The presented work in this article explores the potential of using conductive TPUs as sensors embedded in products such as soft robotics with large deformations, products with structural integrity for life monitoring, and digital twins where the product can provide live feedback.

Author Contributions: Conceptualization, A.R.; methodology, A.R., O.S.N., S.W.E. and M.S.; software, A.R.; validation, A.R.; formal analysis, A.R.; investigation, A.R.; resources, A.R.; data curation, A.R.

and S.W.E.; writing—original draft preparation, A.R., O.S.N., S.W.E. and M.S.; writing—review and editing, O.S.N. and A.R.; visualization, A.R., S.W.E. and O.S.N.; supervision, M.S.; project administration, M.S.; funding acquisition, M.S. All authors have read and agreed to the published version of the manuscript.

Funding: This research received no external funding.

Institutional Review Board Statement: Not applicable.

Data Availability Statement: Data available upon request.

Acknowledgments: We would like to acknowledge the TrollLabs community for supporting with an innovative and exploratory mindset.

Conflicts of Interest: The authors declare no conflicts of interest.

References

1. Kim, S.; Laschi, C.; Trimmer, B. Soft robotics: A bioinspired evolution in robotics. *Cell Press* **2013**, *31*, 1016. [[CrossRef](#)] [[PubMed](#)]
2. Manti, M.; Cacucciolo, V.; Cianchetti, M. Stiffening in Soft Robotics: A Review of the State of the Art. *IEEE Robot. Autom. Mag.* **2016**, *23*, 93–106. [[CrossRef](#)]
3. Zolfagharian, A.; Kouzani, A.Z.; Khoo, S.Y.; Moghadam, A.A.A.; Gibson, I.; Kaynak, A. Evolution of 3D printed soft actuators. *Sens. Actuators Phys.* **2016**, *250*, 258–272. [[CrossRef](#)]
4. Miriyev, A.; Stack, K.; Lipson, H. Soft material for soft actuators. *Nat. Commun.* **2017**, *8*, 596. [[CrossRef](#)] [[PubMed](#)]
5. Gul, J.Z.; Sajid, M.; Rehman, M.M.; Siddiqui, G.U.; Shah, I.; Kim, K.-H.; Lee, J.-W.; Choi, K.H. 3D printing for soft robotics—A review. *Sci. Technol. Adv. Mater.* **2018**, *19*, 243–262. [[CrossRef](#)] [[PubMed](#)]
6. Loepfe, M.; Schumacher, C.M.; Lustenberger, U.B.; Stark, W.J. An Untethered, Jumping Roly-Poly Soft Robot Driven by Combustion. *Soft Robot.* **2015**, *2*, 33–41. [[CrossRef](#)]
7. Whitesides, G.M. Soft Robotics. *Angew. Chem. Int. Ed.* **2018**, *57*, 4258–4273. [[CrossRef](#)] [[PubMed](#)]
8. Mosadegh, B.; Polygerinos, P.; Keplinger, C.; Wennstedt, S.; Shepherd, R.F.; Gupta, U.; Shim, J.; Bertoldi, K.; Walsh, C.J.; Whitesides, G.M. Pneumatic Networks for Soft Robotics that Actuate Rapidly. *Adv. Funct. Mater.* **2014**, *24*, 2163–2170. [[CrossRef](#)]
9. Ilievski, F.; Mazzeo, A.D.; Shepherd, R.F.; Chen, X.; Whitesides, G.M. Soft Robotics for Chemists. *Angew. Chem.* **2011**, *123*, 1930–1935. [[CrossRef](#)]
10. Martinez, R.V.; Fish, C.R.; Chen, X.; Whitesides, G.M. Elastomeric Origami: Programmable Paper-Elastomer Composites as Pneumatic Actuators. *Adv. Funct. Mater.* **2012**, *22*, 1376–1384. [[CrossRef](#)]
11. Walker, J.; Zidek, T.; Harbel, C.; Yoon, S.; Strickland, F.S.; Kumar, S.; Shin, M. Soft Robotics: A Review of Recent Developments of Pneumatic Soft Actuators. *Actuators* **2020**, *9*, 3. [[CrossRef](#)]
12. Polygerinos, P.; Lyne, S.; Wang, Z.; Nicolini, L.F.; Mosadegh, B.; Whitesides, G.M.; Walsh, C.J. Towards a soft pneumatic glove for hand rehabilitation. In Proceedings of the 2013 IEEE/RISJ International Conference on Intelligent Robots and Systems, Tokyo, Japan, 3–7 November 2013; pp. 1512–1517. [[CrossRef](#)]
13. Shepherd, R.F.; Ilievski, F.; Choi, W.; Morin, S.A.; Stokes, A.A.; Mazzeo, A.D.; Chen, X.; Wang, M.; Whitesides, G.M. Multigait soft robot. *Proc. Natl. Acad. Sci. USA* **2011**, *108*, 20400–20403. [[CrossRef](#)] [[PubMed](#)]
14. Sun, Y.; Song, Y.S.; Paik, J. Characterization of silicone rubber based soft pneumatic actuators. In Proceedings of the 2013 IEEE/RISJ International Conference on Intelligent Robots and Systems, Tokyo, Japan, 3–7 November 2013; pp. 4446–4453. [[CrossRef](#)]
15. Park, Y.-L.; Santos, J.; Galloway, K.G.; Goldfield, E.C.; Wood, R.J. A soft wearable robotic device for active knee motions using flat pneumatic artificial muscles. In Proceedings of the 2014 IEEE International Conference on Robotics and Automation (ICRA), Hong Kong, China, 31 May–7 June 2014; pp. 4805–4810. [[CrossRef](#)]
16. Onal, C.D.; Rus, D. A modular approach to soft robots. In Proceedings of the 2012 4th IEEE RAS & EMBS International Conference on Biomedical Robotics and Biomechatronics (BioRob), Rome, Italy, 24–27 June 2012; pp. 1038–1045. [[CrossRef](#)]
17. Martinez, R.V.; Branch, J.L.; Fish, C.R.; Jin, L.; Shepherd, R.F.; Nunes, R.M.D.; Suo, Z.; Whitesides, G.M. Robotic Tentacles with Three-Dimensional Mobility Based on Flexible Elastomers. *Adv. Mater.* **2013**, *25*, 205–212. [[CrossRef](#)] [[PubMed](#)]
18. Marchese, A.D.; Komorowski, K.; Onal, C.D.; Rus, D. Design and control of a soft and continuously deformable 2D robotic manipulation system. In Proceedings of the 2014 IEEE International Conference on Robotics and Automation (ICRA), Hong Kong, China, 31 May–7 June 2014; pp. 2189–2196. [[CrossRef](#)]
19. Gardan, J. Additive manufacturing technologies: State of the art and trends. *Int. J. Prod. Res.* **2016**, *54*, 3118–3132. [[CrossRef](#)]
20. Bikas, H.; Stavropoulos, P.; Chryssolouris, G. Additive manufacturing methods and modelling approaches: A critical review. *Int. J. Adv. Manuf. Technol.* **2016**, *83*, 389–405. [[CrossRef](#)]
21. Singh, S.; Singh, G.; Prakash, C.; Ramakrishna, S. Current status and future directions of fused filament fabrication. *J. Manuf. Process.* **2020**, *55*, 288–306. [[CrossRef](#)]
22. Lalegani Dezaki, M.; Bodaghi, M.; Serjouei, A.; Afazov, S.; Zolfagharian, A. Soft Pneumatic Actuators with Controllable Stiffness by Bio-Inspired Lattice Chambers and Fused Deposition Modeling 3D Printing. *Adv. Eng. Mater.* **2023**, *25*, 2200797. [[CrossRef](#)]

23. Osman, A.; Lu, J. 3D printing of polymer composites to fabricate wearable sensors: A comprehensive review. *Mater. Sci. Eng. R Rep.* **2023**, *154*, 100734. [[CrossRef](#)]
24. Anver, H.M.C.M.; Mutlu, R.; Alici, G. 3D printing of a thin-wall soft and monolithic gripper using fused filament fabrication. In Proceedings of the 2017 IEEE International Conference on Advanced Intelligent Mechatronics (AIM), Munich, Germany, 3–7 July 2017; pp. 442–447. [[CrossRef](#)]
25. Tawk, C.; Mutlu, R.; Alici, G. A 3D Printed Modular Soft Gripper Integrated With Metamaterials for Conformal Grasping. *Front. Robot. AI* **2022**, *8*, 799230. [[CrossRef](#)]
26. Elgeneidy, K.; Neumann, G.; Jackson, M.; Lohse, N. Directly Printable Flexible Strain Sensors for Bending and Contact Feedback of Soft Actuators. *Front. Robot. AI* **2018**, *5*, 00002. [[CrossRef](#)]
27. Yap, H.K.; Ng, H.Y.; Yeow, C.-H. High-Force Soft Printable Pneumatics for Soft Robotic Applications. *Soft Robot.* **2016**, *3*, 144–158. [[CrossRef](#)]
28. Yap, Y.L.; Sing, S.L.; Yeong, W.Y. A review of 3D printing processes and materials for soft robotics. *Rapid Prototyp. J.* **2020**, *26*, 1345–1361. [[CrossRef](#)]
29. Liu, C.; Kim, J.-T.; Yang, D.S.; Cho, D.; Yoo, S.; Madhvapathy, S.R.; Jeong, H.; Yang, T.; Luan, H.; Avila, R. Multifunctional Materials Strategies for Enhanced Safety of Wireless, Skin-Interfaced Bioelectronic Devices. *Adv. Funct. Mater.* **2023**, *33*, 2302256. [[CrossRef](#)]
30. Lee, J.; Cho, D.; Chen, H.; Shim, Y.-S.; Park, J.; Jeon, S. Proximity-field nanopatterning for high-performance chemical and mechanical sensor applications based on 3D nanostructures. *Appl. Phys. Rev.* **2022**, *9*, 011322. [[CrossRef](#)]
31. Wallin, T.J.; Pikul, J.H.; Bodkhe, S.; Peele, B.N.; Mac Murray, B.C.; Therriault, D.; McEnerney, B.W.; Dillon, R.P.; Giannelis, E.P.; Shepherd, R.F. Click chemistry stereolithography for soft robots that self-heal. *J. Mater. Chem. B* **2017**, *5*, 6249–6255. [[CrossRef](#)] [[PubMed](#)]
32. Zhang, N.; Ge, L.; Xu, H.; Zhu, X.; Gu, G. 3D printed, modularized rigid-flexible integrated soft finger actuators for anthropomorphic hands. *Sens. Actuators Phys.* **2020**, *312*, 112090. [[CrossRef](#)]
33. NinjaTek Eel—Technical Datasheet 2018. Available online: <https://ninjatek.com/wp-content/uploads/Eel-TDS.pdf> (accessed on 16 April 2024).
34. NinjaTek Eel—Safety Data Sheet 2018. Available online: https://ninjatek.com/wp-content/uploads/SDS_EEL.pdf (accessed on 20 May 2023).
35. Zolfagharian, A.; Kaynak, A.; Kouzani, A. Closed-loop 4D-printed soft robots. *Mater. Des.* **2020**, *188*, 108411. [[CrossRef](#)]
36. Han, S.-T.; Peng, H.; Sun, Q.; Venkatesh, S.; Chung, K.-S.; Lau, S.C.; Zhou, Y.; Roy, V.A.L. An Overview of the Development of Flexible Sensors. *Adv. Mater.* **2017**, *29*, 1700375. [[CrossRef](#)]
37. Costa, J.C.; Spina, F.; Lugoda, P.; Garcia-Garcia, L.; Roggen, D.; Münzenrieder, N. Flexible Sensors—From Materials to Applications. *Technologies* **2019**, *7*, 35. [[CrossRef](#)]
38. Fan, Z.; Ho, J.C.; Takahashi, T.; Yerushalmi, R.; Takei, K.; Ford, A.C.; Chueh, Y.-L.; Javey, A. Toward the Development of Printable Nanowire Electronics and Sensors. *Adv. Mater.* **2009**, *21*, 3730–3743. [[CrossRef](#)]
39. Suaste-Gómez, E.; Rodríguez-Roldán, G.; Reyes-Cruz, H.; Terán-Jiménez, O. Developing an Ear Prosthesis Fabricated in Polyvinylidene Fluoride by a 3D Printer with Sensory Intrinsic Properties of Pressure and Temperature. *Sensors* **2016**, *16*, 332. [[CrossRef](#)]
40. Bodnicki, M.; Grzybowski, J. Miniature Transducer of Linear Displacement Based on Miniature Hall Effect Sensors. In *Progress in Automation, Robotics and Measuring Techniques*; Szweczyk, R., Zieliński, C., Kaliczynska, M., Eds.; Advances in Intelligent Systems and Computing; Springer International Publishing: Cham, Switzerland, 2015; pp. 21–26. [[CrossRef](#)]
41. Ou, J.; Dublon, G.; Cheng, C.-Y.; Heibeck, F.; Willis, K.; Ishii, H. Cillia: 3D Printed Micro-Pillar Structures for Surface Texture, Actuation and Sensing. In Proceedings of the 2016 CHI Conference on Human Factors in Computing Systems, in CHI'16, San Jose, CA, USA, 7–12 May 2016; Association for Computing Machinery: New York, NY, USA, 2016; pp. 5753–5764. [[CrossRef](#)]
42. Eijking, B.; Sanders, R.; Krijnen, G. Development of whisker inspired 3D multi-material printed flexible tactile sensors. In Proceedings of the 2017 IEEE SENSORS, Glasgow, UK, 29 October–1 November 2017; pp. 1–3. [[CrossRef](#)]
43. Scetta, G.; Selles, N.; Heuillet, P.; Ciccotti, M.; Creton, C. Cyclic fatigue failure of TPU using a crack propagation approach. *Polym. Test.* **2021**, *97*, 107140. [[CrossRef](#)]
44. Georgopoulou, A.; Sebastian, T.; Clemens, F. Thermoplastic elastomer composite filaments for strain sensing applications extruded with a fused deposition modelling 3D printer. *Flex. Print. Electron.* **2020**, *5*, 035002. [[CrossRef](#)]
45. Lawrenson, P.J. Stepping Motors: A Guide to Modern Theory and Practice. *Electron. Power* **1983**, *29*, 659. [[CrossRef](#)]
46. Tung, S.-T.; Yao, Y.; Glisic, B. Sensing sheet: The sensitivity of thin-film full-bridge strain sensors for crack detection and characterization. *Meas. Sci. Technol.* **2014**, *25*, 075602. [[CrossRef](#)]

Disclaimer/Publisher's Note: The statements, opinions and data contained in all publications are solely those of the individual author(s) and contributor(s) and not of MDPI and/or the editor(s). MDPI and/or the editor(s) disclaim responsibility for any injury to people or property resulting from any ideas, methods, instructions or products referred to in the content.